Hyperbola detection with Retinanet: application to new sites and scalability

Tina Wunderlich [1,2*], **Annika Fediuk** [1], **Bente Sven Majchczack** [1,3], **Clemens Mohr** [1,3], **Natalie Pickartz** [4], **Dennis Wilken** [1,2]

1 Institute of Geosciences, Kiel University, Kiel, Germany
2 Collaborative Research Center 1266, Kiel University, Kiel, Germany
3 Cluster of Excellence ROOTS, Kiel University, Kiel, Germany
4 State Office for Cultural Heritage Baden-Württemberg, Ludwigsburg, Germany
* Corresponding author: E-mail: tina.wunderlich@ifg.uni-kiel.de

Abstract
The application of Retinanet to new datasets detected about half of the hyperbola present. Combining the detections from images with different aspect ratios results in better performance. The aspect ratio of the images is a crucial factor for detection.

Keywords
automatization; deep learning; diffraction hyperbola; GPR

Introduction

Machine learning methods became widely used in the last decades in geophysical applications and also in the context of ground penetrating radar (GPR) to automatically detect pipes and rebar or tree roots based on automatic hyperbola picking (e.g. Gamba & Lossani 2000; Shaw et al. 2005; Lei et al. 2019; Liu et al. 2021). From the hyperbolas' shape one can derive the velocity of the electromagnetic waves in the overlying material, which is needed for exact depth determination. Moreover, mapping all hyperbolas on a measured area can result in a map of small objects. In an archaeological context this might provide spatial information on e.g. settlement activity. Manual detection of all hyperbola in a dataset is time-consuming, especially for datasets from multichannel GPR systems containing radargrams up to thousands of kilometers length. In order to automatically detect hyperbolas in radargrams an artificial neural network, Retinanet (Lin et al. 2017a; Lin et al. 2017b), was trained on images from a dataset collected on the island of Föhr, Germany (Wunderlich et al. 2022). After training was completed the network achieved an average precision of 0.58 on data from the same site that was excluded from training. As we only tested data from the same site it was unclear how the network would perform on other data from (a) other sites and (b) collected with other GPR equipment/antenna.

Thus, our main aims of this paper are (1) to check if there is an influence of different aspect ratios of the input images on the detection result, (2) to apply the detection on data from new sites and see how it performs, and (3) to compare the detection results of data from different antenna and GPR systems.

Materials and methods

GPR data collection and processing

The data from Föhr (the training set) was collected with a Mala MIRA 16 channel system with 400 MHz antenna. Further information on processing these data can be found in Wunderlich et al. (2022). The other data in this paper were measured with GSSI systems and 200 and 400 MHz antennas. Processing was done with MultichannelGPR (Wunderlich 2021).

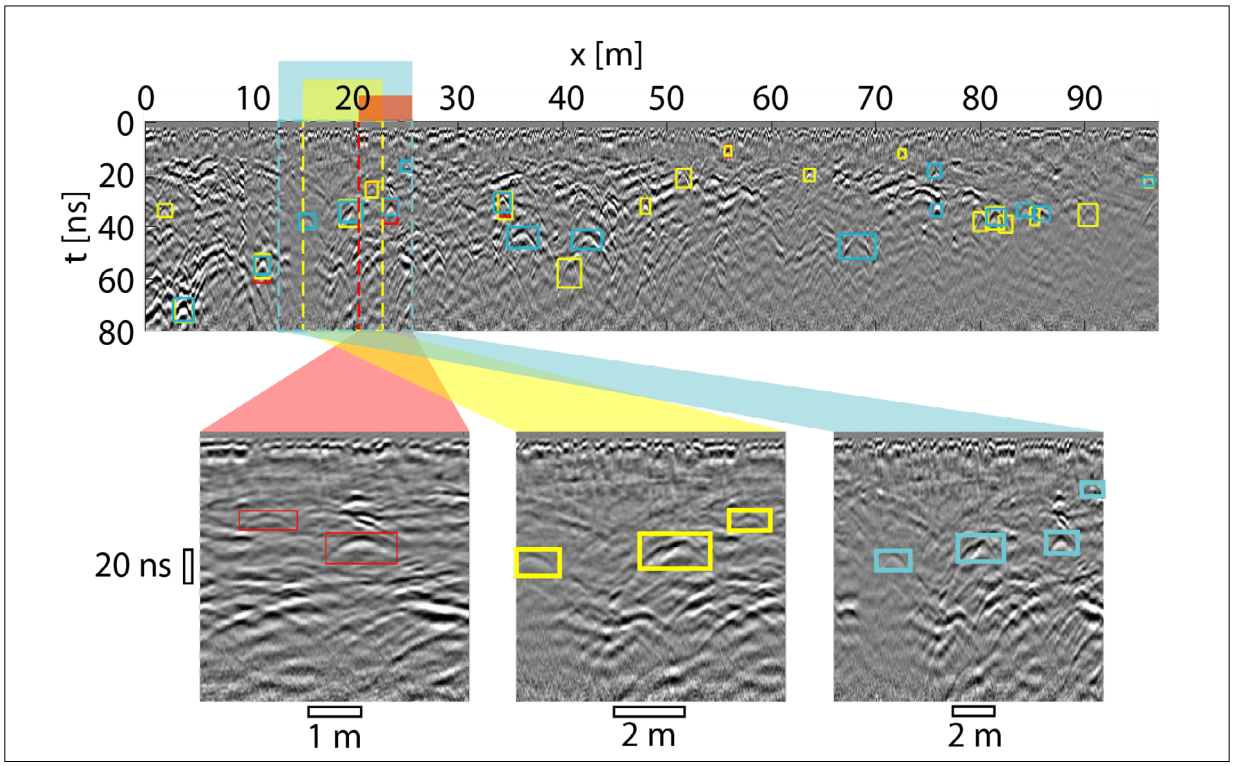

Fig. 1: Example radargram from Föhr with detection results of images with different trace spacings and thus aspect ratios: trace spacing 0.02 m (red), 0.03 m (yellow) and 0.05 m (cyan). The bottom row shows parts of the large radargram that were input images for the network with different aspect ratios.

Hyperbola detection with Retinanet

An existing architecture of Retinanet (Henon 2021) was used with a pretrained ResNet50 as backbone (He et al. 2016). Details can be found in Wunderlich et al. (2022).

Results

The original input images from Föhr for training and testing of our Retinanet had an aspect ratio of 256 * 0.03 m / 80 ns = 0.096 m/ns (with 256 being the number of traces per image and a trace spacing of 0.03m with a time range of 80 ns). Figure 1 shows the detection results on an example radargram for different trace spacings and thus different aspect ratios. The radargram was cut into smaller images of 256 traces using different trace spacings. The different trace spacings were achieved by linear interpolation between the original traces with 0.03 m spacing. This results in different lengths of the images and thus different apparent widths of hyperbola. The original images with 0.03 m trace spacing result in 16 detected hyperbolas in this radargram (Fig. 1, yellow boxes). Decreasing the trace spacing to 0.02 m also decreases the number of detection to 5 (red boxes). An increase of the trace spacing to 0.05 m has the same number of detections (cyan boxes) as for 0.03 m (16), but partly different ones. Thus, combining the detection results of trace spacing 0.03 and 0.05 m results in 27 hyperbolas.

The detection results for the Föhr dataset that was also partly used for training are satisfactory. But what happens for a completely new dataset? For a first test a dataset containing 58 profiles from another archaeological site was chosen, which was measured with a GSSI 200 MHz antenna. The subsurface structure is mainly peat and underneath sand with some timber structures inside the peat layer, which are the origin of the hyperbolas. To take different aspect ratios into account, the trace spacing was varied systematically from 0.01 m to 0.1 m and all images were input into Retinanet. In total 355 hyperbolas are present in all profiles (counted manually = ground truth). For the smallest trace spacing of 0.01 m only one hyperbola was detected (Fig. 2a). Increasing the trace spacing and thus the aspect ratio (Fig. 2b) results in more detections, with a maximum for 0.04 m trace spacing (109 hyperbolas).

KIEL-UP • DOI: https://doi.org/10.38072/978-3-928794-83-1/p91

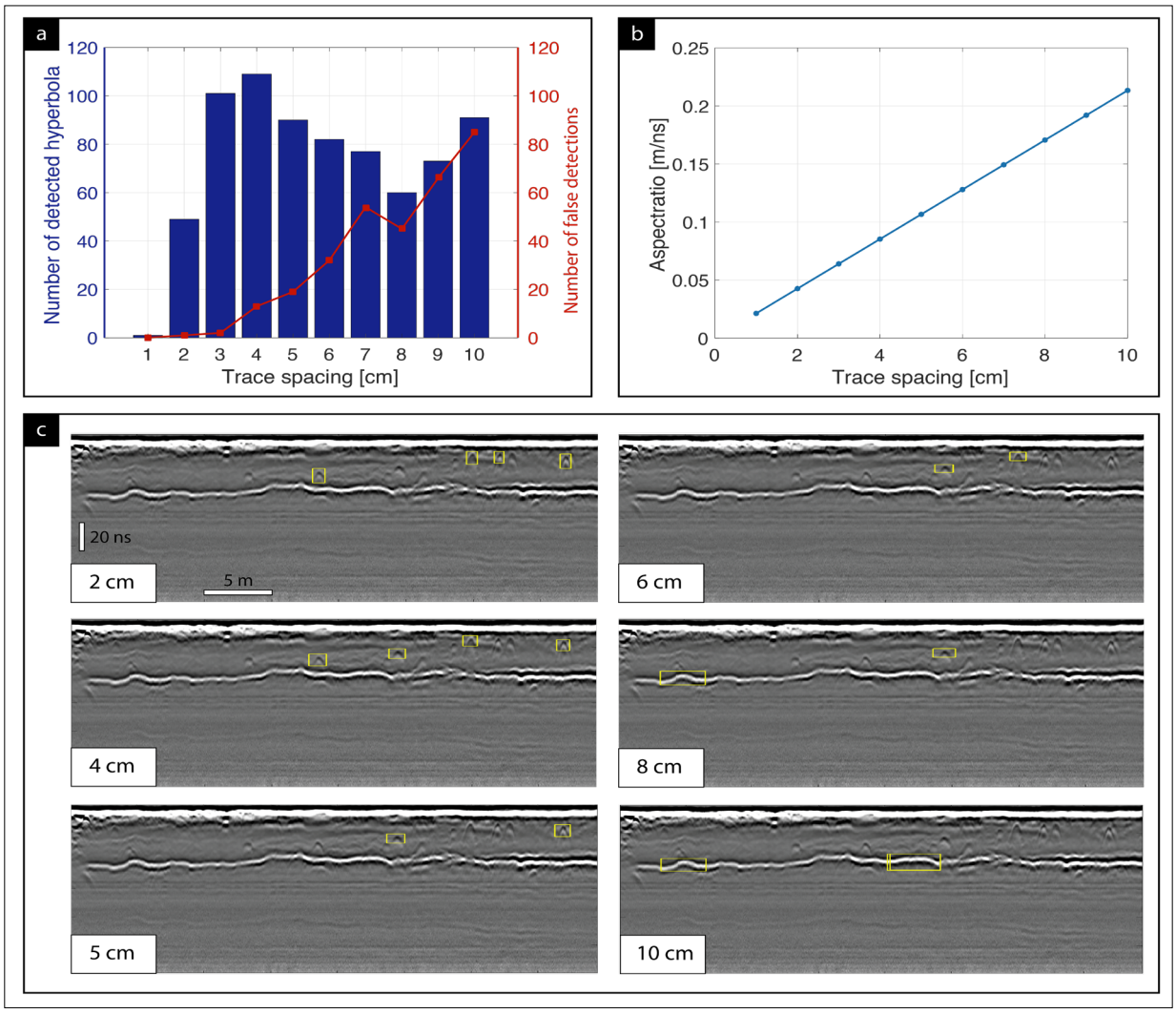

Fig. 2: Application of Retinanet for hyperbola detection on a new dataset from an archaeological site: a) The number of detected hyperbola for different trace spacings together with the number of false detections. b) Aspect ratio versus trace spacing. c) Example radargram and detection results for different trace spacings for the images.

For trace spacings 0.02, 0.04 and 0.05 m the number of detections is similar, but partly different hyperbolas are detected (Fig. 2c), which could be used for increasing the total number of detections when combining both results. For larger trace spacing the number of false detection increases rapidly. This in mainly due to slight curves in the interface reflection that bend upward and are appearing as hyperbolas when the images are compressed horizontally.

For application to other data we did not change the aspect ratio anymore, but chose a ratio similar to the one for the Föhr dataset. For the archaeological dataset measured with a 200 MHz antenna in Figure 3a) the detection resulted in only two hyperbolas. Some hyperbolas in the middle part of the profile with strong chaotic reflections are not detected. In the urban dataset in Figure 3b) again only two pipes are detected and other hyperbolic structures are missed. A special case is the dataset measured from the water surface on a pond with a 400 MHz antenna (Fig. 3c). While most of the image is relatively quiet, two stronger layered reflections are visible and two types of hyperbola: (1) narrow hyperbola in the water (branches and probably fish) and in the bottom of the pond, and (2) very wide hyperbola with long tails revealing a velocity of 30 cm/ns. The latter are caused by trees around the pond and rays travelling trough air. The isolated hyperbola of type 1 are all detected, whereas some below the pond bottom are missed. The wide hyperbola of type 2 are not detected.

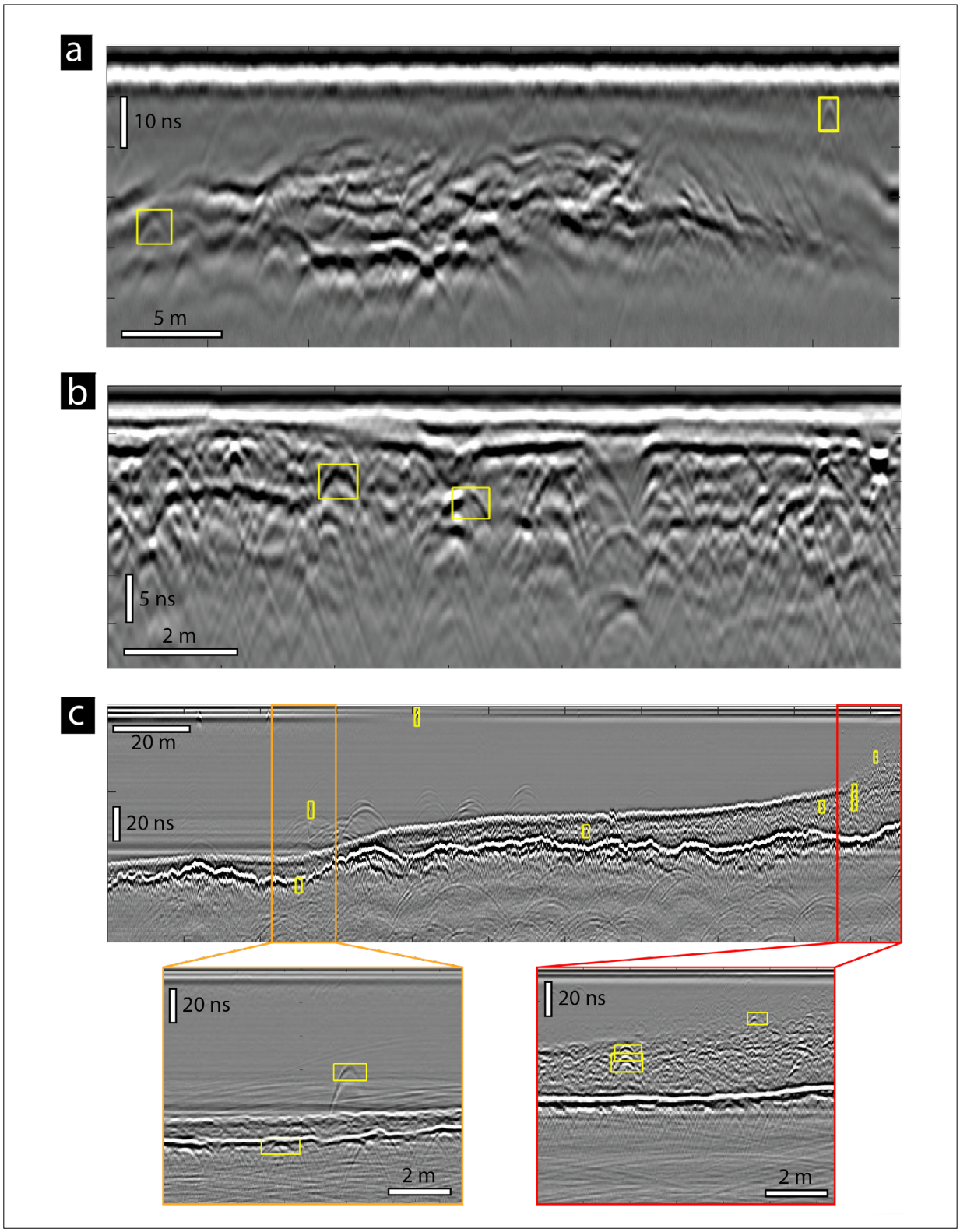

Fig. 3: Hyperbola detection on different example radargrams from new sites and with different equipment: a) Archaeological site, measured with GSSI 200 MHz antenna. b) Urban site, measured with GSSI 400 MHz antenna. c) Pond, measured from the water surface with a GSSI 400 MHz antenna.

KIEL-UP • DOI: https://doi.org/10.38072/978-3-928794-83-1/p91

Discussion and conclusion

The success or failure of the hyperbola detection on new data can be seen in different ways depending on the aim: (1) If one wants to have an overview on all (!) hyperbola present in a dataset for e.g. inferring clusters of objects or counting of subsurface features, the detection performance definitely needs to be increased. (2) If one wants to get a quick automatic look on some hyperbolas and also derive the propagation velocity from them automatically to get a rough velocity model of the site, the detection capability is probably sufficient.

For further training of the network with new data care has to be taken to choose the best aspect ratio. A test should be conducted if it is helpful to include images with many different aspect ratios or to better train the network for one specific aspect ratio. The aspect ratio of new datasets can easily be adjusted by changing the trace spacing with respect to the time range.

With respect to the following automatic velocity determination it is helpful that very wide hyperbola originating from rays travelling through air and being reflected at objects above the surface, are not detected by the Retinanet as it is now.

For new datasets it is helpful to test different aspect ratios of the images in order to detect the 'correct' hyperbola. If the trace spacing gets too large, and thus the aspect ratio too, also slightly curved reflections are 'seen' as hyperbola. As hyperbola in different depths and with different velocities have different widths, it might be also good to infer hyperbolas from images with different aspect ratios and then combine the detection results in order to receive the best performance.

Acknowledgments

This research was funded by the Deutsche Forschungsgemeinschaft (DFG, German Research Foundation, Projektnummer 290391021, "SFB 1266 - Scales of Transformation" and the Priority Program "Harbours" RA 496/26-2).

References

Gamba P, Lossani S. Neural Detection of Pipe Signatures in Ground Penetrating Radar Images. IEEE Trans. Geosci. Remote Sens. 2000;38:790–797. doi: 10.1109/36.842008

He K, Zhang X, Ren S, Sun J. Deep Residual Learning for Image Recognition. In: 2016 IEEE Conference on Computer Vision and Pattern Recognition (CVPR). Las Vegas, NV, USA: IEEE; 2016:770–8. doi: 10.1109/CVPR.2016.90

Henon Y. [Internet] PytorchRetinanet; c2021 [cited 2021 Oct 7]. Available from: https://github.com/yhenon/pytorch-retinanet

Lei W, Hou F, Xi J, Tan Q, Xu M, Jiang X, Liu G, Gu Q. Automatic hyperbola detection and fitting in GPR B-scan image. Autom. Constr. 2019;106:102839. doi: 10.1016/j.autcon.2019.102839

Lin T, Goyal P, Girshick R, He K, Dollár P. Focal loss for dense object detection. Proc. IEEE Int. Conf. Comput. Vis. (ICCV), 2017;2980-2988. doi: 10.48550/ARXIV.1708.02002

Lin T, Dollár P, Girshick R, He K, Hariharan B, Belongie S. Feature Pyramid Networks for Object Detection. 2017 IEEE Conference on Computer Vision and Pattern Recognition (CVPR), 2017;936-944. doi: 10.1109/CVPR.2017.106

Liu Z, WuW, Gu X, Li S, Wang L, Zhang T. Application of Combining YOLO Models and 3D GPR Images in Road Detection and Maintenance. Remote Sens. 2021;13:1081. doi: 10.3390/rs13061081

Shaw MR, Millard SG, Molyneaux TCK, Taylor MJ, Bungey JH. Location of steel reinforcement in concrete using ground penetrating radar and neural networks. NDTE Int. 2005;38:203–212. doi: 10.1016/j.ndteint.2004.06.011

Wunderlich T, Wilken D, Majchczack BS, Segschneider M, Rabbel W. Hyperbola Detection with RetinaNet and Comparison of Hyperbola Fitting Methods in GPR Data from an Archaeological Site. Remote Sens. 2022;14:3665. doi: 10.3390/rs14153665

Wunderlich T. MultichannelGPR – A New MATLAB-Tool for the Processing of GPR Data, ArcheoSciences 2021;45(1):279-283. doi: 10.4000/archeosciences.10100